Finite-Element Simulation of Stratified Multiphase Flows

The analysis of stratified multiphase flow fields is difficult because the position of the interface is unknown *a priori* and there is a discontinuity in the normal viscous stress and/or pressure at the interface. A finite-element technique that uses double nodes along the interface has been implemented. The immiscible liquid displacement in a capillary tube was examined in detail. Fountain flow in the advancing fluid, reverse fountain flow in the receding fluid, and a recirculating flow region in the less viscous fluid were determined. In Newtonian flat film coextrusion the entry region, where the two immiscible fluids form an interface, and the characteristic swelling and bending of the extrudate at the die exit were studied. The computational results compare favorably with available experimental observations.

H. Mavridis, A. N. Hrymak, and J. Vlachopoulos
Department of Chemical Engineering
McMaster University
Hamilton, Ontario, Canada L8S4L7

Introduction

In stratified multiphase flow problems two or more components form continuous phases that are separated from each other by continuous boundaries (interfaces). This type of flow occurs frequently in engineering applications: in polymer processing (bicomponent fiber, multilayer flat film, coextruded cables and wires; Han, 1981), multilayer coating (Kistler and Scriven, 1984), and in oil recovery by immiscible displacement through porous media (Dussan, 1977). The common characteristic of all these processes is the existence of one or more interfaces whose position is unknown *a priori* (free surface problem). Interfaces bounded by solid boundaries introduce the additional complexity of the static or dynamic contact line (Dussan, 1979). Also, the understanding of instabilities associated with multilayer flows is limited (Han, 1981; Joseph et al., 1984a,b), and the design of processing equipment is largely based on a trial-and-error procedure.

Despite their importance, there has been little progress on the solution of general interface problems. The unknown interface location results in a nonlinear problem and an analytical solution is impossible for all but very simple cases.

The finite-element approach has been successful for free boundary problems due to the ability of the elements to take the shape of the free surface and to handle complex boundaries. Many free boundary problems have been solved so far with the finite-element method; for example, extrudate swell by Nickell et al. (1974), coating flows by Kistler and Scriven (1984), calendering by Mitsoulis et al. (1985). However, in all of the above cases the free surface was part of the external boundary of the fluid domain. For interface problems there are additional complexities due to a pressure discontinuity and normal viscous stress jumps. The discontinuity arises due to the finite jump in the fluid properties at the interface, since the interface is modeled as a surface with zero thickness. The discontinuity invalidates the continuous approximation adopted by a standard application of the finite-element method and requires a special treatment.

The purpose of this paper is to advocate such a technique and form a methodology for stratified multiphase flow problems. The technique allows the finite-element grid itself to be discontinuous at the interface by having two values for the primitive variables (velocities and pressure) on two different nodes at the same spatial location. Primitive variables that are continuous are specified as such, interface boundary conditions are applied directly, and the finite jump in the discontinuous variables is determined from the solution of the global system.

This double-node finite-element method has been used as a standard technique to handle discontinuities in other areas of computational mechanics: in fracture mechanics for crack problems (Mirza and Olson, 1978; Liaw et al., 1984), and especially in aerodynamics for inviscid flow over airfoils (Baskharone and Hamed, 1981; Cox et al., 1982). It was also applied to incompressible viscous flow, namely two-layer curtain coating, by Kistler (1984). Recently Dheur and Crochet (1986) proposed a different method to handle the pressure discontinuity in stratified multiphase flows by employing a C^{-1} pressure approximation (i.e., discontinuous pressure at interelement boundaries).

The discussion involves the implementation of the method, and we present three example problems that demonstrate the strength of the approach. The first problem is the immiscible displacement of two viscous fluids inside a capillary that generates a recirculating flow in a bolus at the interface (Dussan, 1977). The second problem involves the merging of two Newtonian streams in a flat die geometry. An analytical solution for fully developed flow (Whitaker, 1968) is used to check the accuracy of the computed solution. The third problem is the coextrusion of two Newtonian fluids. Extrudate bending is predicted and its dependence on the viscosity ratio is in agreement with the experimentally observed trend (Southern and Ballman, 1973, 1975, 1979).

Normal Viscous Stress and Pressure Discontinuity at Interfaces

Consider the flow of two immiscible fluids denoted by *I* and *II* in Figure 1. The two flow fields are governed by the Navier-Stokes equations and are coupled through the boundary conditions along the interface. Referring to a local coordinate system (tangential t and normal n to the interface) the boundary conditions at the interface are expressed as:

Kinematic condition

$$V_{t,I} = V_{t,II} \tag{1}$$

$$V_{n,I} = V_{n,II} = 0 \tag{2}$$

Tangential stress condition

$$\mu_I\left(\frac{\partial V_{t,I}}{\partial n} + \frac{\partial V_{n,I}}{\partial t}\right) = \mu_{II}\left(\frac{\partial V_{t,II}}{\partial n} + \frac{\partial V_{n,II}}{\partial t}\right) \tag{3}$$

Normal stress condition

$$-P_I + 2\mu_I\frac{\partial V_{n,I}}{\partial n} = -P_{II} + 2\mu_{II}\frac{\partial V_{n,II}}{\partial n} + \frac{2H}{Ca} \tag{4}$$

where

$Ca = \mu_* V_*/\gamma_*$ = capillary number (* denotes reference value)
$2H$ = mean surface curvature
P_I, P_{II} = pressure of fluids *I* and *II* at the interface

(Equation 3 implies the absence of tangential surface tension gradients, which could be caused by temperature gradients or surfactants.)

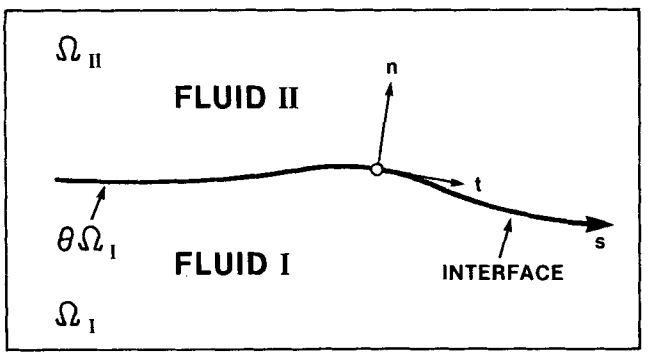

Figure 1. Diagram of a fluid-fluid interface.

A discontinuity in pressure arises, under certain conditions, at the interface. For incompressible fluids the continuity equation may be written as:

Fluid I

$$\frac{\partial V_{t,I}}{\partial t} + \frac{\partial V_{n,I}}{\partial n} = 0 \tag{5}$$

Fluid II

$$\frac{\partial V_{t,II}}{\partial t} + \frac{\partial V_{n,II}}{\partial n} = 0 \tag{6}$$

From Eq. 1 we have:

$$\frac{\partial V_{t,I}}{\partial t} = \frac{\partial V_{t,II}}{\partial t} = \frac{\partial V_t}{\partial t} \tag{7}$$

Combining Eqs. 5 and 6 and using Eq. 7:

$$\frac{\partial V_{n,I}}{\partial n} = \frac{\partial V_{n,II}}{\partial n} = -\frac{\partial V_t}{\partial t} \tag{8}$$

The normal stress condition may be written as:

$$(P_{II} - P_I) = 2(\mu_I - \mu_{II})\frac{\partial V_t}{\partial t} + \frac{2H}{Ca} \tag{9}$$

By examining Eq. 9, we conclude that there will be a pressure discontinuity:

1. Whenever there are nonnegligible surface tension effects ($2H/Ca \neq 0$).
2. In the absence of surface tension effects ($2H/Ca = 0$) but with viscosities of the two fluids being different ($\mu_I - \mu_{II} \neq 0$). In this case the pressure discontinuity will be proportional to the tangential velocity gradient ($\partial V_t/\partial t$).

Double-Node Finite-Element Technique

The governing equations for steady, isothermal flow of an incompressible fluid include the conservation of linear momentum and the mass continuity equation:

$$\nabla \cdot \sigma - V \cdot \nabla V + g = 0 \tag{10a}$$

$$\nabla \cdot V = 0 \tag{10b}$$

where σ is the total stress tensor, $\sigma = -PI + \tau$.

The Galerkin finite-element *u-v-p* formulation of the above system proceeds by expanding the unknown velocity and pressure fields in a suitable set of basis functions:

$$V = \sum_i N_i^v V_i \tag{11a}$$

$$P = \sum_i N_i^p P_i \tag{11b}$$

where Vi, P_i are nodal variables, N_i^v basis functions for velocity, and N_i^p basis functions for pressure. The basis functions are localized (nonzero only over a small portion of the flow domain)

low-order polynomials, defined over small subdomains, the elements. The approximations, Eqs. 11a,b, are inserted into Eqs. 10a,b. The resulting momentum residuals are weighted with the velocity basis functions and the continuity residuals are weighted with the pressure basis functions. The weighted residuals are integrated over the solution domain and set to zero, i.e.:

$$\boldsymbol{R}_i^m = \int_\Omega (\nabla \cdot \boldsymbol{\sigma} - \boldsymbol{V} \cdot \nabla \boldsymbol{V} + \boldsymbol{g}) N_i^v \, d\Omega = 0 \qquad (12a)$$

$$R_i^c = \int_\Omega \nabla \cdot \boldsymbol{V} N_i^p \, d\Omega = 0 \qquad (12b)$$

The stress term in Eq. 12a is integrated by parts (i.e., applying the divergence theorem):

$$\boldsymbol{R}_i^m = \int_\Omega (\nabla N_i^v \cdot \boldsymbol{\sigma} + N_i^v \boldsymbol{V} \cdot \nabla \boldsymbol{V} - N_i^v \boldsymbol{g}) d\Omega - \int_{\partial\Omega} \boldsymbol{n} \cdot \boldsymbol{\sigma} N_i^v \, ds = 0 \qquad (12c)$$

Note that in this formulation the dynamic (stress) boundary conditions arise naturally as boundary integrals in the momentum residuals.

Equations 12b and 12c, when applied at the nodes of the discretized flow domain along with the appropriate boundary conditions, provide as many equations as there are unknown nodal velocity and pressure variables.

For free surface problems the free surface location is not known *a priori*. It is possible to include the free surface location as an additional unknown, expand in a suitable set of basis functions as in Eqs. 11a,b, and iterate simultaneously with the flow field. In this work the free surface location is decoupled and treated separately from the flow field.

It should be noted that in the approximations in Eqs. 11a,b it is tacitly assumed that the field variables are continuous over the solution domain. It may be possible to approximate the discontinuity by using a fine mesh near the interface. However, the continuous approximation is totally inappropriate when surface tension effects are significant. In these cases, not only the pressure but also the normal viscous stress on the interface is discontinuous.

A way of handling the above-mentioned discontinuity is to allow the finite-element grid itself to be discontinuous, i.e., have two values for the primitive variables (velocities and pressure) on two different nodes at the same spatial location (double nodes along the interface). Consider again the interface in Figure 1 separating two immiscible fluids *I* and *II* and a pair of nodes at the same spatial location. Equations 12b and 12c apply in the two flow domains Ω_I and Ω_{II}, while at the interface the boundary conditions in full vector form are:

Kinematic

$$\boldsymbol{V}_I = \boldsymbol{V}_{II}, \quad (\boldsymbol{n} \cdot \boldsymbol{V})_I = (\boldsymbol{n} \cdot \boldsymbol{V})_{II} = 0 \qquad (13a)$$

Dynamic

$$(\boldsymbol{n} \cdot \boldsymbol{\sigma})_I = (\boldsymbol{n} \cdot \boldsymbol{\sigma})_{II} + \frac{1}{Ca} \frac{d\boldsymbol{t}_I}{ds} \qquad (13b)$$

where $\boldsymbol{t}_I$ is the tangential vector in the direction of increasing s.

The momentum residuals at the double nodes will be:

$$\boldsymbol{R}_{i,I}^m = \int_{\Omega_I} (\nabla N_i^v \cdot \boldsymbol{\sigma}_I + N_i^v \boldsymbol{V}_I \cdot \nabla \boldsymbol{V}_I - N_i^v \boldsymbol{g}) d\Omega - \int_{\partial\Omega_I} (\boldsymbol{n} \cdot \boldsymbol{\sigma})_I N_i^v \, ds \qquad (14a)$$

$$\boldsymbol{R}_{i,II}^m = \int_{\Omega_{II}} (\nabla N_i^v \cdot \boldsymbol{\sigma}_{II} + N_i^v \boldsymbol{V}_{II} \cdot \nabla \boldsymbol{V}_{II} - N_i^v \boldsymbol{g}) d\Omega - \int_{\partial\Omega_{II}} (\boldsymbol{n} \cdot \boldsymbol{\sigma})_{II} N_i^v \, ds \qquad (14b)$$

Combination of the momentum residuals, Eqs. 14a and 14b, at the double nodes and use of the dynamic boundary condition, Eq. 13b, gives:

$$\boldsymbol{R}_i^m = \boldsymbol{R}_{i,I}^m + \boldsymbol{R}_{i,II}^m = \int_{\Omega_I} (\nabla N_i^v \cdot \boldsymbol{\sigma}_I + N_i^v \boldsymbol{V}_I \cdot \nabla \boldsymbol{V}_I - N_i^v \boldsymbol{g}) d\Omega + \int_{\Omega_{II}} (\nabla N_i^v \cdot \boldsymbol{\sigma}_{II} + N_i^v \boldsymbol{V}_{II} \cdot \nabla \boldsymbol{V}_{II} - N_i^v \boldsymbol{g}) d\Omega - \frac{1}{Ca} \int_{\partial\Omega_I} \frac{d\boldsymbol{t}_I}{ds} N_i^v \, ds = 0 \qquad (15a)$$

The pressure involved in the total stress tensor $\boldsymbol{\sigma}$ is discontinuous at the interface. Since the pressure is a Lagrange multiplier introduced to satisfy the incompressibility constraint, the continuity residuals must be weighted with the pressure basis functions separately on either side of the interface, i.e.:

$$R_{i,I}^c = \int_{\Omega_I} \nabla \cdot \boldsymbol{V}_I N_i^p \, d\Omega = 0 \qquad (15b)$$

$$R_{i,II}^c = \int_{\Omega_{II}} \nabla \cdot \boldsymbol{V}_{II} N_i^p \, d\Omega = 0 \qquad (15c)$$

The two scalar equations resulting from the vector equation, Eq. 15a, and Eqs. 15b and 15c provide four equations corresponding to the four variables at the interface nodes (two velocity components and two pressure variables). Although separate nodal variables (velocities and pressure) are defined at both the double nodes, the imposition of the kinematic condition for continuity of the velocity field at the interface eliminates the second velocity degree of freedom (i.e., only the pressure is double-valued at the interface nodes). With this technique, the system is closed, interface boundary conditions are used to match the two flow fields, and the pressure discontinuity is determined from the solution of the global system. The unknown free surface location is treated separately, as will be shown below.

Implementation of the Method in Finite-Element Codes

The interface position is unknown *a priori* and must be determined with the flow field as a solution to the governing nonlinear partial differential equations. The resulting free boundary problem is usually solved using one of two different iteration procedures, Picard-like, or Newton-Raphson.

Picard-like Iteration. In this case the flow field and the free

surface are "decoupled" through an iteration of the form:

$$X_{FF}^{i+1} = f_1(X_{FF}^{i}, X_{FS}^{i}) \tag{16}$$

$$X_{FS}^{i+1} = f_2(X_{FF}^{i+1}, X_{FS}^{i}) \tag{17}$$

where

X_{FF} = flow field degrees of freedom (i.e., u-v-p)
X_{FS} = free-surface degrees of freedom
i = iteration number
f_1, f_2 = governing equations and boundary conditions (and any additional constraints, e.g., dynamic contact angle for moving contact line problems)

The crucial step in the above procedure is the seleciton of the f_2 function, i.e., the selection of the autonomous equation on which the iteration is based. This procedure has the advantages of simplicity and a large radius of convergence. Oscillatory and slow convergence are the usual drawbacks, but they can be eliminated by a proper convergence promotion method.

Newton-Raphson Iteration. In this case the complete system of Eqs. 16 and 17 is assembled and the problem is solved with the Newton-Raphson method. Quadratic convergence and availability of the Jacobian matrix (which provides information about the sensitivity of the solution and ill-conditioning of the global system) are the advantages of this approach. Small radius of convergence and scaling problems are potential difficulties.

The method of Picard-like iteration was used in this work. However, the double-node technique is equally well suited for both methods.

Double-Node Technique and Picard-like Iteration

The free surface iteration is based on the function f_2 in Eq. 17. It is well known (Silliman and Scriven, 1980) that the proper choice of f_2 is the kinematic boundary condition when viscous effects are dominant and the normal stress boundary condition when surface tension effects are dominant. In either case the corresponding boundary condition is relaxed, a free surface location is chosen on the basis of previous iterations, and the system is solved with the remaining boundary conditions. The residual in the relaxed boundary condition is then used to update the free surface between successive iterations.

In both cases the finite-element grid is constructed with double nodes on the interface, as shown in Figure 2. This figure also shows a fictitious pressure distribution (vertical axis) exhibiting a discontinuity at the interface and how the double nodes are used to capture this discontinuity.

The iteration procedures must be modified, as follows:

Kinematic Iteration. Continuity of both the normal and tangential stress is imposed with iteration on the kinematic boundary condition (i.e., the kinematic boundary condition is relaxed on the free surface). The former is obtained by simply assigning the same global variable number for the two local velocity degrees of freedom at the double nodes on the interface (surface tension effects are neglected).

Normal Stress Iteration. Continuity of the tangential stress and zero normal velocity are imposed with iteration on the normal stress boundary condition (i.e., the normal stress boundary condition is relaxed on the free surface). Applying nodal transformation, as described by Engelman et al. (1982), the global x-y coordinate system is transformed to a local n-t (normal and tangential to the interface) coordinate system at each node on the free surface. The normal and tangential vectors (needed for

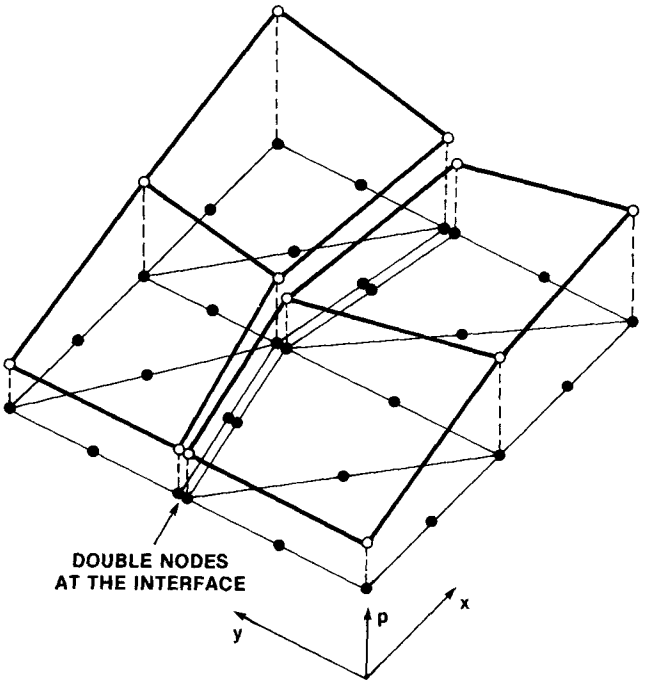

Figure 2. Diagram of a discontinuous grid illustrating pressure discontinuity (vertical axis).

the transformation) at the corners of linear elements are determined uniquely by the requirement of mass conservation. Continuity of the tangential stress is applied by assigning the same global variable number for the two t-velocity degrees of freedom at the double nodes on the interface. Zero normal velocity is imposed by setting to zero the two n-velocity degrees of freedom at the double nodes.

In both iterative methods, the pressure is left discontinuous at the double nodes and is determined by the solution of the global system.

The above procedures are equivalent to combining the momentum residuals at the double nodes on the interface so as to satisfy all but the relaxed interfacial boundary conditions while the mass continuity residuals are defined on either side of the interface, allowing the pressure discontinuity.

It is readily seen that the double-node technique with Picard-like free surface iteration can easily be adapted, with only minor modifications, to any finite-element code based on the primitive variable formulation of the Navier-Stokes equations. However, there is a point concerning the type of equation solver to be used (band or frontal solver). If a band solver, or any other solver that operates on a nodal basis and assembles the global system before any elimination, is used, then there is no problem and the technique is applied directly. If a frontal solver is used, care must be taken in the assembly-elimination procedure, since the frontal solver operates on an elemental basis and the double nodes would appear unrelated. A typical frontal solver, that of Taylor and Hughes (1981), eliminates the variables at the last appearance of each node. This would fail at the double nodes unless some provision has been taken to ensure that no continuous variable is eliminated before all contributions to both the double nodes have been completed. Otherwise, large front width and meaningless solution (usually in the pressure) results. In this work the frontal solver was used, properly modified for the

assembly-elimination of equations corresponding to variables at the double nodes.

Example Problems

The double-node technique has been applied to three different problems. Each has an interface with the aforementioned discontinuity, but the problems are sufficiently different from one another that having an internal boundary parametrized with double nodes is the key to efficient solution.

The immiscible liquid displacement problem has a discontinuity due to surface tension and viscosity difference, with the additional complication of a moving contact line. The normal stress iterative scheme is used.

The other two problems are specific cases of coextrusion. They do not involve surface tension effects (the kinematic iterative scheme is used) but have large viscosity differences that cause an interfacial pressure discontinuity. The complicating features include extrudate swelling and bending at the exit.

The creeping flow assumption is made for all cases, so that the governing equations reduce to:

Momentum

$$-\nabla P + \nabla \cdot \tau = 0 \tag{18}$$

Continuity

$$\nabla \cdot V = 0 \tag{19}$$

The appropriate boundary conditions are given specifically for each problem in subsequent sections.

Triangular elements are used with basis functions that are quadratic for velocities and linear for pressure. Details of the derivation of the discretized equations are available elsewhere (Huebner and Thornton, 1982).

Streamlines are calculated *a posteriori* by solving the equation:

$$\frac{\partial^2 \Psi}{\partial x^2} + \frac{\partial^2 \Psi}{\partial y^2} = -\omega, \text{ planar flow} \tag{20a}$$

$$\frac{\partial}{\partial r}\left(\frac{1}{r}\frac{\partial \Psi}{\partial r}\right) + \frac{\partial}{\partial z}\left(\frac{1}{r}\frac{\partial \Psi}{\partial z}\right) = -\omega, \text{ axisymmetric flow} \tag{20b}$$

where the stream function and the vorticity are defined as:

Cartesian coordinates

$$V_x = \frac{\partial \Psi}{\partial y}, \quad V_y = -\frac{\partial \Psi}{\partial x} \tag{21}$$

$$\omega = \frac{\partial V_y}{\partial x} - \frac{\partial V_x}{\partial y} \tag{22}$$

Cylindrical coordinates

$$V_r = \frac{1}{r}\frac{\partial \Psi}{\partial z}, \quad V_z = -\frac{1}{r}\frac{\partial \Psi}{\partial r} \tag{23}$$

$$\omega = \frac{\partial V_z}{\partial r} - \frac{\partial V_r}{\partial z} \tag{24}$$

The vorticity is available from the solution of the Navier-Stokes system. The same grid is used for the finite-element solution of Eqs. 20a,b with quadratic basis functions for the stream function.

Immiscible liquid displacement in a capillary tube

When two immiscible fluids displace each other inside a capillary a toroidal-like flow occurs adjacent to the moving interface. The resulting flow field is schematically shown in Figure 3, where a viscous fluid (lower fluid) advances upward, displacing a less viscous fluid at constant speed. The frame of reference is at rest with respect to the moving interface so that the walls appear to move downward with the velocity of the advancing interface. The advancing fluid undergoes fountain flow (Rose, 1961; Mavridis et al., 1986), the receding fluid undergoes reverse fountain flow, and a bolus forms inside the less viscous fluid so as to meet the requirements of mass continuity and compatibility between the two flow fields. The existence of the bolus was first observed and documented experimentally by Dussan (1977), who injected dye on the interface and noticed that a portion of it was trapped and recirculating next to the interface, inside the less viscous fluid.

This phenomenon is of interest for oil recovery by immiscible displacement through porous media. It is common practice to introduce surfactants to reduce surface tension and enhance oil recovery. Therefore, it is important whether the surfactants remain on the interface or are pushed off and forced away from it (Dussan, 1977).

A review of the relevant literature can be found in Kafka and Dussan (1979), with an analytical solution for the limiting case of a flat interface, and a detailed discussion of the phenomena near the contact line. Also, Huh and Scriven (1971) solved the problem of a flat interface moving over a solid plane and

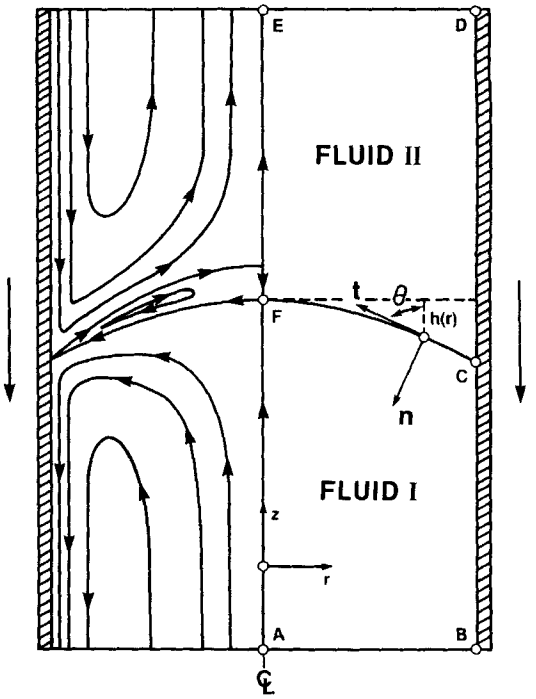

Figure 3. Diagram of flow domain for immiscible liquid displacement problem.

obtained analytically the characteristic streamline pattern in the vicinity of the contact line. Contact line is the intersection of the interface with the wall. Contact angle is the angle that the moving interface forms with the wall (dynamic contact angle). The hydrodynamics in the vicinity of the contact line and the factors affecting the contact angle are still open questions. The continuum approach, along with the no-slip boundary condition, results in a nonintegrable singularity at the moving contact line (infinite drag on the wall; Huh and Scriven, 1971; Dussan, 1976).

Numerical Simulation. Consider the steady creeping flow motion of a viscous fluid *I* inside a capillary displacing a less viscous fluid *II*, as shown in Figure 3. The frame of reference is at rest with respect to the interface. Characteristic scales used to define dimensionless quantities are the velocity of the interface V_{avg}, the viscosity of the more viscous fluid μ_I, the tube radius R, and the quantity $\mu_I V_{avg}/R$ for stress.

The following boundary conditions were used:

$$\text{On } AB \quad V_r = 0, \quad \boldsymbol{nn}:\boldsymbol{\sigma} = P_{AB} \tag{25a}$$

$$\text{On } BC, CD \quad V_r = 0, \quad V_z = -1 \tag{25b}$$

$$\text{At the contact line, point } C \quad V_r = 0, \quad V_z = 0 \tag{25c}$$

$$\text{On } ED \quad V_r = 0, \quad \boldsymbol{nn}:\boldsymbol{\sigma} = 0 \tag{25d}$$

$$\text{On } EFA \quad V_r = 0, \quad \boldsymbol{tn}:\boldsymbol{\sigma} = 0 \tag{25e}$$

$$\text{and on the interface, } FC \quad V_r, V_z \text{ continuous}, \quad \boldsymbol{n}\cdot\boldsymbol{V} = 0 \tag{25f}$$

$$(\boldsymbol{tn}:\boldsymbol{\sigma})_{II} = (\boldsymbol{tn}:\boldsymbol{\sigma})_I \tag{25g}$$

$$(\boldsymbol{nn}:\boldsymbol{\sigma})_{II} = (\boldsymbol{nn}:\boldsymbol{\sigma})_I + 2H/Ca \tag{25h}$$

The choice of the above set of boundary conditions is not obvious and there are important points to note:

1. The boundary condition at the contact line, Eq. 25c, introduces an artificial slip at the element adjacent to the contact line (Kistler and Scriven, 1984). It may be possible to use an equation relating the slip velocity to the local tangential stress (Silliman and Scriven, 1980). However such an approach is equally arbitrary and involves an additional parameter, the characteristic slip length. Very little is known about the mechanism of the moving contact line and both approaches are aimed at alleviating the stress singularity there. A common numerical approach is the use of a very fine grid near the singular point to reduce the error originating at the contact line.

2. The boundary condition of Eq. 25d sets the pressure level in fluid *II*. However, since the pressure is discontinuous at the interface the boundary condition, Eq. 25a was used to set the pressure level in fluid *I*. The constant P_{AB} appearing in Eq. 25a is an additional unknown and requires an additional equation. This is provided by a force balance on the interface (Appendix A) which, for nonvanishing surface tension effects, involves the apparent dynamic contact angle. The system is not closed until this angle, θ_c in Eq. A7, is given. Lowndes (1980) chose θ_c to be the static contact angle and he defined a measured contact angle using the equation:

$$\theta_M = \cos^{-1}\frac{2h(1)}{1+h^2(1)} \tag{26}$$

Equation 26 is derived on the basis of the assumption that the interface is a segment of a sphere. Another definition of a dynamic contact angle is given by West's (1911) equation (also Kafka and Dussan, 1979):

$$P(-L_I) - P(L_{II}) = 8\left(L_I + \frac{\mu_{II}}{\mu_I}L_{II}\right) + \frac{2}{Ca}\cos\theta_W \tag{27}$$

This equation gives the pressure drop between two points, L_I upstream (advancing fluid) and L_{II} downstream (receding fluid) from the contact line, and is based on two assumptions:

1. Both fluids undergo Poiseuille flow up to the contact line
2. The pressure drop across the interface is given by the same formula used under static conditions.

Equation 27 was used in this work to obtain starting values of P_{AB}, where θ_M was used in place of θ_W. The wetting fliud was the less viscous one (fluid *II*) and the viscosity ratio was 0.1. The angle θ_c was fixed at 80° and the capillary number was varied in the range 10^{-3}–10^{-1}.

The interface was parametrized with double nodes and the normal stress iterative scheme was used, as described in Appendix A. Zero-order continuation was applied, i.e., the converged solution for one value of the capillary number was used as an initial estimate for the next value of the *Ca*. This iterative scheme gave converged solutions within five iterations for *Ca* up to 0.1. The failure to obtain converged solutions iterating on the normal stress condition in cases where surface tension effects are no longer dominant is consistent with the findings of Silliman and Scriven (1980).

Consider a typical case, for $Ca = 0.01$. The finite-element grid used is shown in Figure 4. The computed flow field is shown in Figure 5, where the more viscous fluid is on the lower part and advances upward. The velocity vectors are plotted on the right

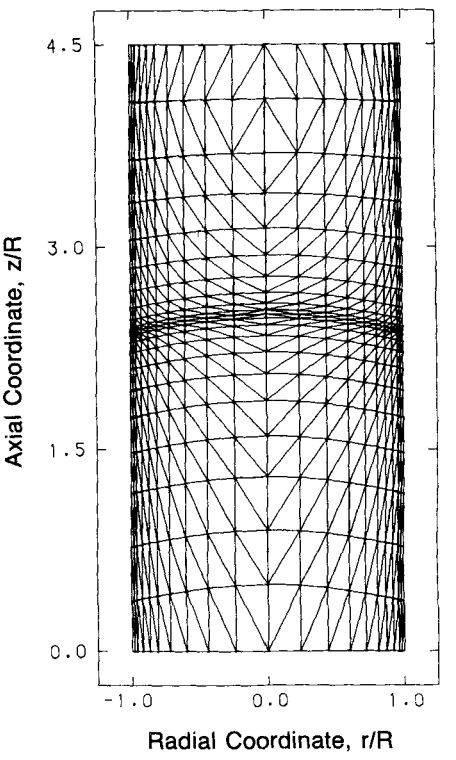

Figure 4. Finite-element grid.

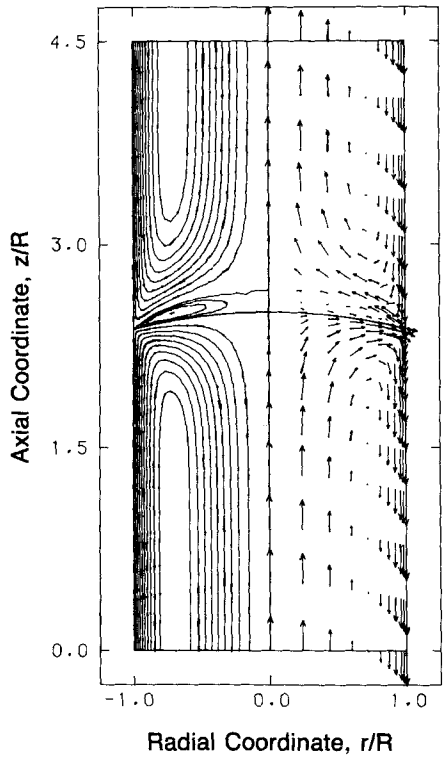

Figure 5. Velocity vectors and streamlines.
The more viscous fluid is on the lower part; Ca = 0.01; viscosity ratio = 0.1; θ_c = 80°

half and the streamlines on the symmetric left half. This figure clearly shows the advancing fluid undergoing fountain flow, the receding fluid undergoing reverse fountain flow, and the characteristic vortex next to the interface inside the less viscous fluid, fully in agreement with the work of Dussan (1977) and Kafka and Dussan (1979).

The discontinuity of the pressure at the interface that necessitated the use of a special finite-element technique is shown in Figure 6, which is a plot of the pressure along the centerline.

The effect of the capillary number Ca on the interface shape is shown in Figure 7. As Ca is increased, that is, as the effect of the viscous terms is increased, the interface deviates more from the limiting static case, becoming more convex.

A stagnation point appears at the intersection of the interface with the centerline. As a result of the vortex formation a second stagnation point appears on the centerline, inside the less viscous fluid. The normalized distance Z_{st} between the two stagnation points is a measure of the size of the vortex, while the relative rate of fluid recirculating in the vortex Ψ_v is a measure of its intensity. The dependence of Z_{st} and Ψ_v on Ca is given in Table 1. It is shown that the vortex becomes smaller in size and weaker in intensity as Ca is increased.

Table 1 also gives a comparison of our calculated pressure drop ΔP_{cal} and that calculated through West's equation, Eq. 27, ΔP_{th} where θ_M was used in place of θ_W. The angle θ_M was calculated from Eq. 26 and it is also given in the table. It is seen that the agreement is surprisingly good considering the simplifying assumptions on which West's equation is based. In fact, experience on numerical work has shown that pressure drops calculated from equations derived on the basis of a lubrication-like approximation are usually accurate for engineering calculations. However, pressure drop alone provides no information on the flow field and the solution of the full equations is needed for this purpose.

Coextrusion problem

Coextrusion is a process commonly used in the polymer industry by which different melt streams are combined to produce multilayer composite films and fibers. We are concerned here with the flat film coextrusion case, assuming a thin film so that the flow can be described as two-dimensional. We distinguish two flow regions: the die entry region where the different layers meet and form the interface, and the die exit region. It is well known that the layers in the exiting stream have different thicknesses from those inside the die (extrudate swell) and the viscosity mismatch results in different swelling ratios. Therefore, efficient methods for the analysis and design of the process are crucial for an economically successful operation. It is shown below how the double-node finite-element technique can be used to solve these problems.

Die Entry Region. The flow domain to be considered is shown in Figure 8. Two Newtonian fluids are fed from the two arms of

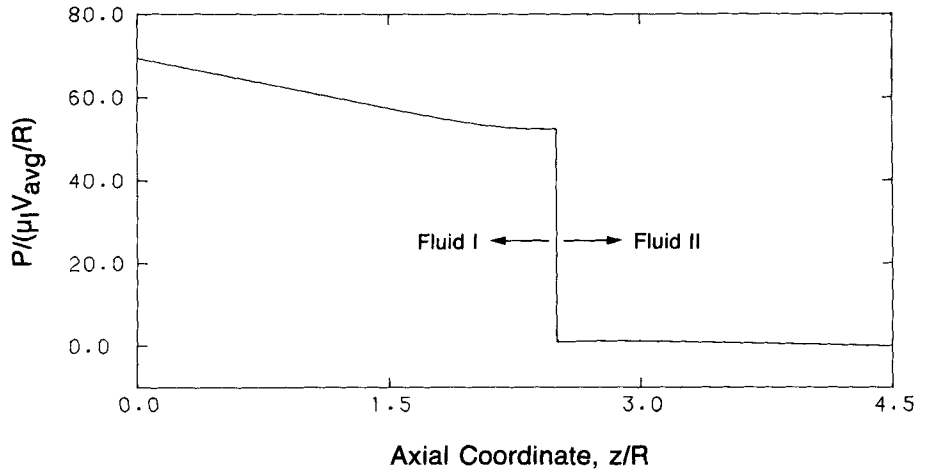

Figure 6. Pressure along the centerline.
Parameters as in Figure 5

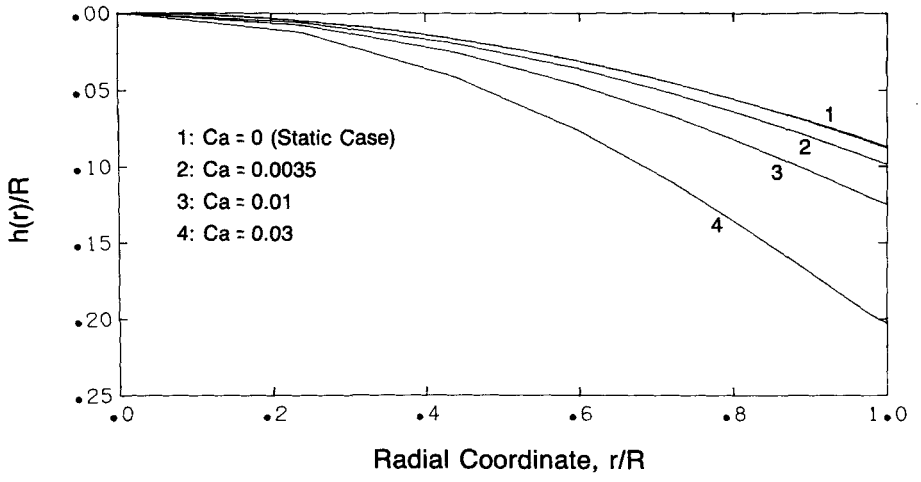

Figure 7. Interface shape dependence on capillary number.
Viscosity ratio = 0.1, $\theta_c = 80°$

the die at a given flow rate ratio. The interface starts forming at point G and develops downstream. An analytical expression is available for the interface location and the velocity profile in fully developed flow (Whitaker, 1968), thereby providing a means for checking the numerically derived solution. Characteristic scales used to define dimensionless quantities are the maximum velocity of the entering more viscous fluid V_{max}, the viscosity of the more viscous fluid μ_I, the die halfwidth D, and the quantity $\mu_I V_{max}/D$ for stress.

The boundary conditions for this problem are:
Vanishing normal velocity and no-slip at solid boundaries:

$$\text{On } AB, ED, \text{ and } FGH \quad \boldsymbol{n} \cdot \boldsymbol{V} = 0, \quad \boldsymbol{t} \cdot \boldsymbol{V} = 0 \tag{28a}$$

$$\text{On } BCD \quad \boldsymbol{nn}\colon \boldsymbol{\sigma} = 0, \quad \boldsymbol{t} \cdot \boldsymbol{V} = 0 \tag{28b}$$

Note that the above boundary condition sets the pressure level in both fluids.

$$\text{On } AH \quad (\boldsymbol{n} \cdot \boldsymbol{V})_I = f_I(x, y), \quad (\boldsymbol{t} \cdot \boldsymbol{V})_I = 0 \tag{28c}$$

$$\text{On } EF \quad (\boldsymbol{n} \cdot \boldsymbol{V})_{II} = f_{II}(x, y), \quad (\boldsymbol{t} \cdot \boldsymbol{V})_{II} = 0 \tag{28d}$$

The functions f_I and f_{II} give the velocity profiles for Newtonian Poiseuille flow and are defined such that:

$$\frac{\int_{EF} (\boldsymbol{n} \cdot \boldsymbol{V})_{II} ds}{\int_{AH} (\boldsymbol{n} \cdot \boldsymbol{V})_I ds} = \frac{Q_{II}}{Q_I} = q \tag{28e}$$

where q is the flow rate ratio.

Table 1. Results for Immiscible Liquid Displacement Problem

Ca	$h(1)$	Z_{st}	Ψ_v	ΔP_{calc}	Θ_M	ΔP_{th}
0.001	0.0884	0.1767	0.0614	382.62	79.9	371.82
0.0035	0.0987	0.1711	0.0596	134.39	78.73	132.60
0.01	0.1250	0.1573	0.0546	69.46	75.75	69.93
0.03	0.2028	0.1162	0.0436	45.17	67.05	46.14
0.06	0.3177	0.0697	0.0296	37.93	54.75	38.55
0.1	0.5040	0.0169	0.0129	34.08	36.04	34.14

$$\text{On the interface } GC \quad V_x, V_y \text{ continuous}, \quad \boldsymbol{n} \cdot \boldsymbol{V} = 0 \tag{28f}$$

$$(\boldsymbol{tn}\colon \boldsymbol{\sigma})_I = (\boldsymbol{tn}\colon \boldsymbol{\sigma})_{II} \tag{28g}$$

$$(\boldsymbol{nn}\colon \boldsymbol{\sigma})_I = (\boldsymbol{nn}\colon \boldsymbol{\sigma})_{II} \tag{28h}$$

For a given viscosity ratio and flow rate ratio the system is closed. The solution proceeds by parametrizing the interface with double nodes and iterating on the kinematic boundary condition, since surface tension effects are neglected. The iterative scheme used for this case is described in Appendix B. The viscosity ratio was varied in the range 0.2–1.0 and the flow rate ratio in the range of 0.125–8.0. Converged solutions were obtained within five to ten iterations, with convergence being slower for high flow rate ratios. It should also be noted that direct application of the Picard-like iteration:

$$\boldsymbol{x}^{i+1} = \boldsymbol{f}(\boldsymbol{x}^i) \tag{29}$$

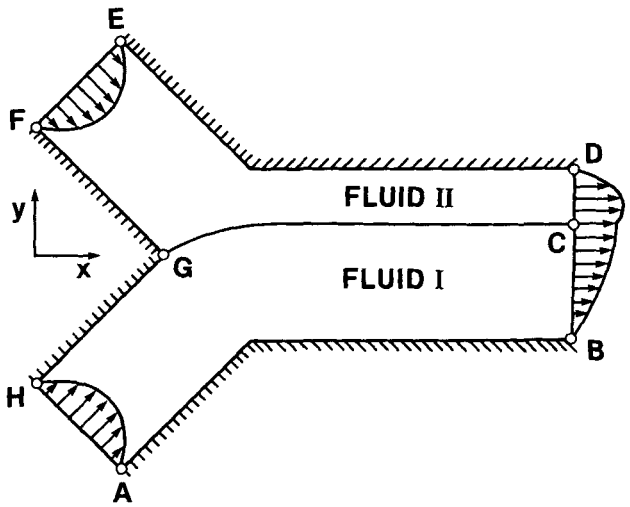

Figure 8. Diagram of flow domain for coextrusion problem (entry region).

diverged. Therefore, an underrelaxation scheme was employed:

$$x^{i+1} = x^i + \lambda[f(x^i) - x^i] \tag{30}$$

where λ is the relaxation factor. Numerical experiments have shown that a value of $\lambda = 0.5$ worked well for this problem.

The finite-element grid used for a typical case of $\mu_{II}/\mu_I = 0.2$, $Q_{II}/Q_I = 1$ is shown in Figure 9a. The computed velocity vectors are given in Figure 9b and the streamlines in the vicinity of the interface in Figure 9c. The interface develops smoothly, exhibiting an overshoot, as shown in Figure 9c, of approximately 20% of the final value, for this case. The pressure discontinuity at the interface is shown in Figure 10, where it is plotted vs. the tangential velocity gradient $\partial V_t/\partial t$. As discussed earlier (Eq. 9), in the absence of surface tension effects the resulting curve of $P_{II} - P_I$ vs. $\partial V_t/\partial t$ must be a straight line with slope $2(\mu_I - \mu_{II})$ and zero intercept [for $\mu_{II}/\mu_I = 0.2$, $2(\mu_I - \mu_{II}) = 1.6$]. It is seen in Figure 10 that this is true except in the vicinity of the static contact line (point G in Figure 8 and upper right part in Figure 10) where the solution is singular due to the no-slip boundary condition. The tangential velocity gradient and the pressure discontinuity are zero in the fully developed region. This plot also indicates that the error originating at the static contact line decays quickly, approximately over two elements. The data points in Figure 10 correspond to element corner nodes at the interface.

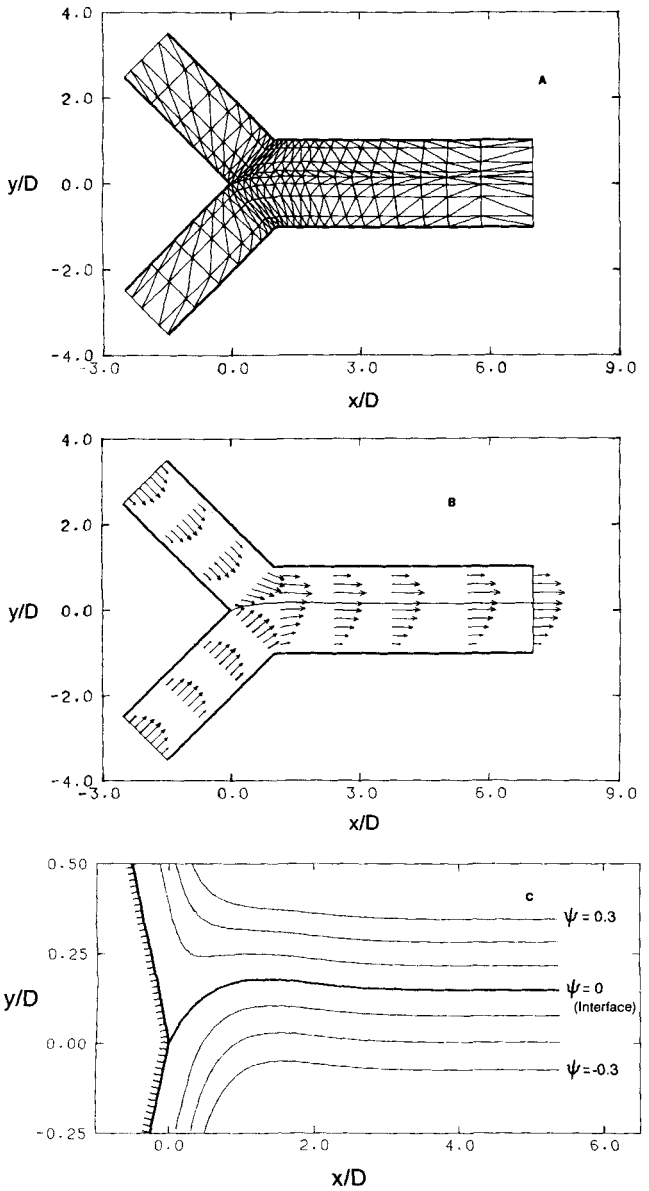

Figure 9. Coextrusion problem, entry region ($Q_{II}/Q_I = 1$, $\mu_{II}/\mu_I = 0.2$).
a. Finite element grid
b. Velocity vectors
c. Streamlines in vicinity of interface; vertical scale exaggerated by a factor of five

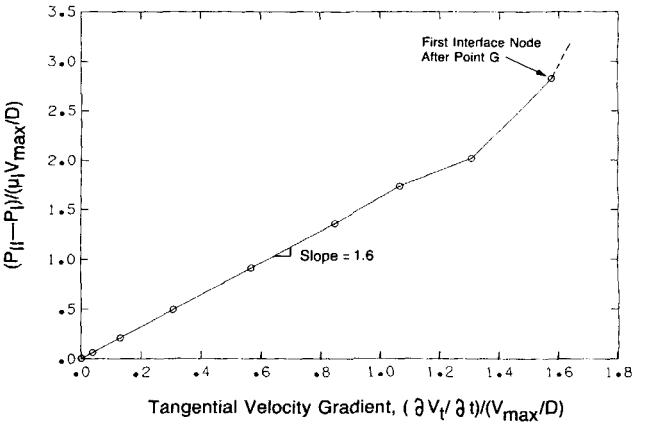

Figure 10. Coextrusion problem, entry region.
Pressure discontinuity at interface vs. tangential velocity gradient, parameters as in Figure 9

The calculated interface location ℓ in the fully developed region (downstream) is compared to the analytically derived solution in Table 2. The relative error in the computed velocity profile was in the range 10^{-2}–10^{-4}.

Die Exit Region. In a typical polymeric film production operation the extrudate is drawn by a wind-up mechanism downstream. The draw ratio D_R, defined as the ratio of the wind-up velocity over the mean extrusion velocity, is adjusted so as to reduce the film thickness at the desired value. This process is known as film or sheet casting (Middleman, 1977) and it is the two-dimensional counterpart of the fiber spinning process (Denn, 1983). Finite-element computations for the single-layer film casting process have been presented by Kistler (1984).

The interesting feature with two-layer films is the bending of the extrudate at low draw ratios, as shown schematically in Fig-

Table 2. Numerical and Analytical Solutions for Interface Location in Fully Developed Flow Region ($\mu_{II}/\mu_I = 0.2$)

Q_{II}/Q_I	ℓ numerical*	ℓ analytical**	Error %
0.125	0.6981	0.69286	−0.76
0.25	0.5442	0.53906	−0.95
0.5	0.3520	0.34999	−0.57
1.0	0.1482	0.14699	−0.82
2.0	−0.05078	−0.05074	−0.077
4.0	−0.2336	−0.23202	−0.68
8.0	−0.4042†	−0.39153	−3.24†

*Tolerance = 0.01
**From Whitaker (1968)
†After 10 iterations

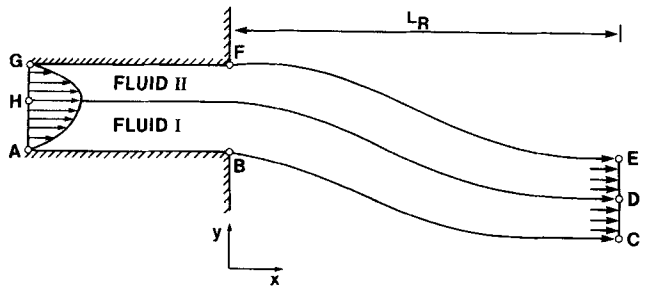

Figure 11. Diagram of flow domain for coextrusion problem (exit region).

ure 11. The bending always occurs toward the more viscous fluid as a result of the viscosity mismatch; the less viscous fluid moves faster and therefore the rates of velocity change will be different for the two fluids in the die exit region. An unequal rate of velocity change results in a net force directed toward the more viscous fluid, thereby causing bending of the exit stream. Extrudate bending was observed experimentally by Southern and Ballman (1973, 1975, 1979) in side-by-side coextrusion from a tube. They defined an extrudate exit angle as the angle between the extrudate and the tube centerline, and found that it was increasing with the viscosity ratio.

We consider here the two-dimensional case as depicted in Figure 11. A wind-up mechanism is assumed at some distance L_R from the die exit, such that it exerts a force in the x direction only and it is free to translate in the y direction. A plug velocity profile is assumed at the downstream boundary and either the draw ratio or the drawing force must be specified. For a given draw ratio, flow rate ratio, and viscosity ratio the problem can be solved with the following boundary conditions (referring to Figure 11):

$$\text{On } AB, FG \quad \boldsymbol{n} \cdot \boldsymbol{V} = 0, \quad \boldsymbol{t} \cdot \boldsymbol{V} = 0 \tag{31a}$$

$$\text{On } AH, HG \quad \text{analogous to Eqs. 28c–28d} \tag{31b}$$

Note that the upstream interface location, point H, is known.

$$\text{On } FE, BC \quad \boldsymbol{n} \cdot \boldsymbol{V} = 0, \quad \boldsymbol{tn}\colon \boldsymbol{\sigma} = 0, \quad \boldsymbol{nn}\colon \boldsymbol{\sigma} = 0 \tag{31c}$$

$$\text{On } HD \text{ (interface)} \quad V_x, V_y \text{ continuous}, \quad \boldsymbol{n} \cdot \boldsymbol{V} = 0 \tag{31d}$$

$$(\boldsymbol{tn}\colon \boldsymbol{\sigma})_I = (\boldsymbol{tn}\colon \boldsymbol{\sigma})_{II} \tag{31e}$$

$$(\boldsymbol{nn}\colon \boldsymbol{\sigma})_I = (\boldsymbol{nn}\colon \boldsymbol{\sigma})_{II} \tag{31f}$$

$$\text{On } CD, DE \quad V_x = D_R(Q_I + Q_{II})/2D, \quad V_y = 0 \tag{31g}$$

In this problem not only the interface but also the upper and lower free surfaces (lines HD, FE, and BC in Figure 11) are unknown. Solution was obtained through the kinematic iteration procedure. The interface was parametrized with double nodes and the kinematic boundary condition was relaxed on the interface, the upper and lower free surfaces. Free surface locations were updated between successive iterations as described in Appendix B.

In the absence of the downstream drawing force and for a viscosity ratio equal to unity, the problem reduces to the Newtonian extrudate swell, which has become a benchmark for free boundary solvers. The swelling ratio, defined as the ratio of the extrudate thickness over the die thickness, is the quantity being checked. Crochet and Keunings (1982), who studied the effect of mesh refinement on the computed swelling ratio, reported a value of 19.6%, while coarse meshes resulted in higher values. The limit of 19.6% was also verified by Mitsoulis et al. (1984). For more details on this problem the reader is referred to a recent textbook by Tanner (1985). With the finite-element grid used in the present study the computed swelling ratio was 20%, which was considered acceptable as a trade-off between accuracy and computer time. It should also be noted that the effect of grid density is more profound for the case of multilayer flows. For a viscosity ratio equal to unity and a flow rate equal to unity (i.e., single fluid with the interface on the centerline) it was found that when the grid density was different in the two layers a small asymmetry was observed in the calculated upper and lower free surface location. This is attributed to the nonsymmetrical dispersion of the error in the solution domain.

Calculations were performed for a draw ratio D_R fixed to unity, flow rate ratio Q_{II}/Q_I equal to unity, and a length $L_R/D = 20$. The viscosity ratio μ_{II}/μ_I was varied in the range 0.4–1.0. The underrelaxation scheme of Eq. 30 was necessary and convergence was slow (10–15 iterations).

The finite-element grid used for a typical case, $\mu_{II}/\mu_I = 0.5$, is shown in Figure 12a. The computed velocity field is given in Figure 12b. The lower fluid is the more viscous one. It is seen that upon emerging from the die the velocity rearrangement causes a stream bending toward the more viscous fluid. Eventually the extrudate becomes parallel to the centerline due to the axial drawing force.

Although an extrudate exit angle is not unambiguously defined for this system, it can be associated with the vertical deflection of the exit stream from the inflow direction. The effect of the viscosity ratio on the extrudate deflection is shown in Figure 13. For equal viscosities the flow is symmetric about the centerline. As the viscosity ratio is decreased the extrudate bends toward the high-viscosity component, deflecting more from the centerline. These results agree with the experimental observations of Southern and Ballman (1973, 1975, 1979). Although elastic polymers were involved in their experiments, it appears from the present calculations that extrudate bending is caused by the viscosity mismatch.

Concluding Remarks

A double-node finite-element technique has been implemented for stratified multiphase flow problems. Using this method three different problems were examined: immiscible liquid displacement in a capillary tube, merging of two immiscible streams, and extrusion of Newtonian bicomponent films. It became possible to determine free surface and interface location using an iterative scheme for u-v-p formulation of the Navier-Stokes system.

For the immiscible liquid displacement problem a recirculating bolus at the interface was predicted, in agreement with experimental observations (Dussan, 1977), and an asymptotic analytical solution (Kafka and Dussan, 1979). Pressure drop and interface shape dependence on the capillary number were determined.

The interface position in the fully developed region, for the stream merging problem, was calculated and compared to an analytical solution. Pressure discontinuity and tangential veloc-

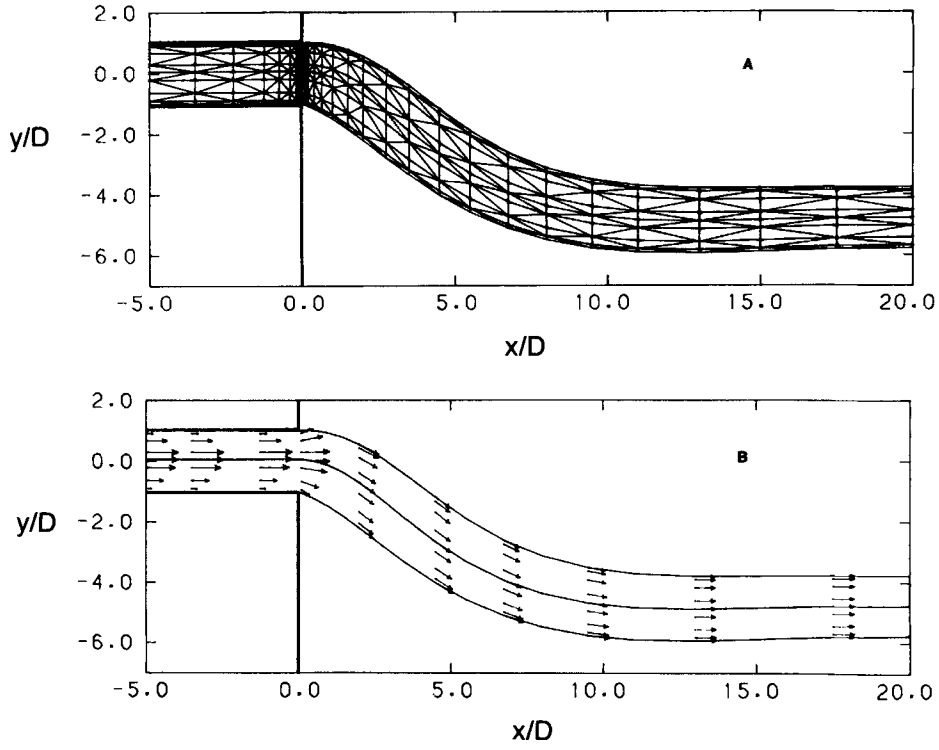

Figure 12. Coextrusion problem, exit region ($Q_{II}/Q_I = 1$, $\mu_{II}/\mu_I = 0.5$, $D_R = 1$).
a. Finite element grid
b. Velocity vectors

ity gradient at the interface were calculated and their relationship was compared to the linear one predicted by theory.

Extrudate bending was predicted for plane coextrusion of Newtonian fluids. Decreasing the viscosity ratio increases the extrudate bending, as was found experimentally by Southern and Ballman (1973, 1975, 1979) in a similar problem.

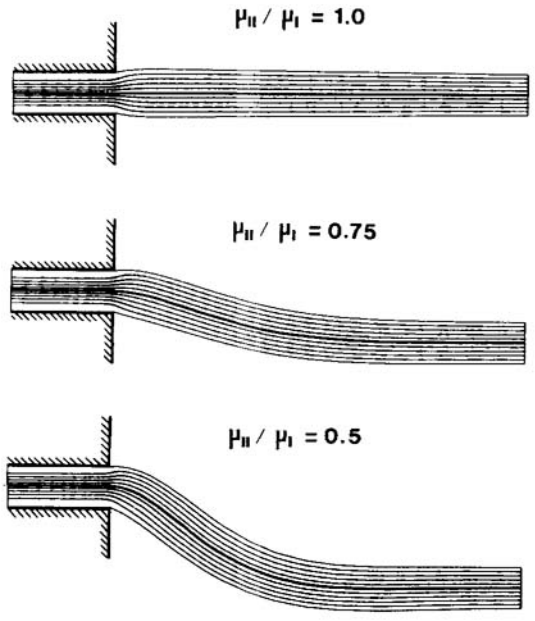

Figure 13. Coextrusion problem, exit region.
Effect of viscosity ratio on extrudate bending ($Q_{II}/Q_I = 1$, $D_R = 1$)

Acknowledgment

Financial assistance from the Natural Sciences and Engineering Research Council of Canada is gratefully acknowledged. H. Mavridis was also the recipient of a Shell Canada Graduate Research Fellowship.

Notation

Ca = capillary number, (velocity)(viscosity)/surface tension
D = die halfwidth
D_R = draw ratio
f = function
g = body force vector
H = mean surface curvature
$h(x)$ = free surface position as a function of the x coordinate
$h(r)$ = interface position as a function of radius
i = unit vector in the x direction
j = unit vector in the y direction
ℓ = dimensionless interface distance from centerplane, distance/halfwidth
L = length
L_R = distance of wind-up mechanism from die exit
n = local coordinate normal to the interface
n = outward normal vector
N_i^p = basis function for pressure
N_i^v = basis function for velocities
P = pressure
Q = flow rate per unit width
R = tube radius
r = radial coordinate
R_i^c = continuity residual
R_i^m = momentum residual
s = local coordinate on the boundary surface
t = local coordinate tangential to the interface
t = tangential vector
u = x or r velocity component
v = y or z velocity component
V = velocity vector

V_{avg} = average velocity of fluid I
V_{max} = maximum velocity of fluid I at the inflow plane
x = x coordinate
$\boldsymbol{x}$ = vector of discretized variables
y = y coordinate
z = axial coordinate
Z_{st} = distance between stagnation points

Greek letters

γ = surface tension
θ_c = apparent dynamic contact angle, Eq. A7
θ_M = measure contact angle, Eq. 26
θ_W = apparent dynamic contact angle, Eq. 27
λ = relaxation factor, Eq. 30
μ = viscosity
σ = total stress tensor, $\sigma = -Ip + \tau$
τ = deviatoric stress tensor, $\tau = \mu(\nabla V + \nabla V^T)$
Ψ = stream function, Eqs. 21 and 23
Ψ_v = vortex intensity
ω = vorticity, Eqs. 22 and 24
Ω = solution domain
$\partial\Omega$ = boundary surface

Superscripts

c = continuity
i = iteration number
m = momentum

Subscripts

i = quantity associated with the ith node
n = component normal to the interface
r = r component
t = component tangential to the interface
x = x component
y = y component
z = z component
I = more viscous fluid
II = less viscous fluid

Appendix A: Normal Stress Iterative Scheme for the Immiscible Liquid Displacement Problem

The normal stress iterative scheme used is a modification of that proposed by Lowndes (1980) in a similar problem. The mean surface curvature of the interface in Figure 3 can be expressed as:

$$-2H = \frac{d^2h/dr^2}{[1 + (dh/dr)^2]^{3/2}} + \frac{1}{r}\frac{dh/dr}{[1 + (dh/dr)^2]^{1/2}} \quad \text{(A1)}$$

If θ denotes the angle, at a given value of r, between a line tangent to the interface and the wall then:

$$-\frac{dh}{dr} = \cot\theta \quad \text{(A2)}$$

and Eq. A1 can be rewritten as:

$$2H = \frac{1}{r}\frac{d}{dr}(r\cos\theta) \quad \text{(A3)}$$

The normal stress boundary condition Eq. 25h is:

$$(\boldsymbol{nn}\colon\sigma)_{II} = (\boldsymbol{nn}\colon\sigma)_I + \frac{1}{Ca}\frac{1}{r}\frac{d}{dr}(r\cos\theta) \quad \text{(A4)}$$

Integrating Eqs. A2 and A4 with respect to r and using the boundary conditions that $h = 0$ and $\cos\theta = 0$ at $r = 0$, we obtain:

$$-h(r) = \int_0^r \cot\theta\, dr' \quad \text{(A5)}$$

$$\cos\theta = \frac{Ca}{r}\int_0^r [(\boldsymbol{nn}\colon\sigma)_{II} - (\boldsymbol{nn}\colon\sigma)_I]r'\, dr' \quad \text{(A6)}$$

Equations A5 and A6 form the basis of the iterative scheme:

1. Guess an interface profile and a value for P_{AB} in Eq. 25a
2. Discretize the flow domain with double nodes on the interface
3. Solve the governing equations with boundary condition Eqs. 25a–25g
4. Update the interface profile $h(r)$ and the pressure P_{AB} as follows:

P_{AB} Update. From Eq. A6 and for $r = 1$ we obtain

$$\cos\theta_c = Ca\int_0^1 [(\boldsymbol{nn}\colon\sigma)_{II} - (\boldsymbol{nn}\colon\sigma)_I]r'\, dr' \quad \text{(A7)}$$

The above is an equation for P_{AB} involved in $(\boldsymbol{nn}\colon\sigma)_I$. The angle θ_c is assumed known. It may be different from, and it does not force the dynamic contact angle to have specified value but merely imposes a net interfacial force at the contact line (Lowndes, 1980; Bach and Hassager, 1985).

Interface Update. The new P_{AB} value is used to correct the $(\boldsymbol{nn}\colon\sigma)_I$ values and the new interface shape is determined from Eq. A5 by numerical integration. The values of the angle θ at the integration points are calculated from Eq. A6.

The iterations proceed until the maximum relative update is less than a predefined tolerance (10^{-3}).

Appendix B: Kinematic Iterative Scheme

The kinematic iterative scheme will be derived for the interface shown in Figure 9. The interface, line GC, can be parametrized as the elevation $h(x)$ above the x axis. The normal vector on the interface is:

$$\boldsymbol{n} = \frac{1}{\sqrt{1 + (dh/dx)^2}}\left(-\frac{dh}{dx}\boldsymbol{i} + \boldsymbol{j}\right) \quad \text{(B1)}$$

The kinematic boundary condition is:

$$\boldsymbol{n}\cdot\boldsymbol{V} = 0 \quad \text{(B2)}$$

Substituting Eq. B1 in Eq. B2:

$$-V_x\frac{dh}{dx} + V_y = 0$$

or

$$h(x_2) - h(x_1) = \int_{x_1}^{x_2}\frac{V_y}{V_x}dx \quad \text{(B3)}$$

and $h(0) = 0$ for this case. Equation B3 is the basis of the itera-

tive scheme, which proceeds as follows:

1. Construct an interface profile on the basis of the previous iteration (for the first iteration guess one)

2. Discretize the flow domain with double nodes on the interface

3. Solve the problem relaxing the kinematic boundary condition, Eq. B2

4. Update the interface profile using Eq. B3, if the maximum relative change is greater than a small tolerance go to step 1.

This iterative scheme was first proposed by Nickell et al. (1974) and Tanner et al. (1975), and it is equivalent to constructing a new free streamline at every iteration. They employed Simpson's rule to carry out the integration in Eq. B3 over each element (using two corners and the midside node). However, the ratio V_y/V_x is singular at the contact line (element corner node). In this work, Gaussian quadrature is used, which is an open-end formula and avoids the above singularity.

Literature cited

Bach, P., and O. Hassager, "An Algorithm for the Use of the Lagrangian Specification in Newtonian Fluid Mechanics and Applications to Free-Surface Flow," *J. Fluid Mech.*, **152,** 173 (1985).

Baskharone, E., and A. Hamed, "A New Approach in Cascade Flow Analysis Using the Finite-Element Method," *AIAA J.*, **19,** 65 (1981).

Cox, G. L., G. J. Fix, and M. D. Gunzburger, "A Least-Squares Finite-Element Scheme for Transonic Flow Around Harmonically Oscillating Wings," Rept. No. 19, ICASE NASA Langley Research Center, Hampton, VA (1982).

Crochet, M. J., and R. Keunings, "On Numerical Die Swell Calculation," *J. Non-Newt. Fluid Mech.*, **10,** 85 (1982).

Denn, M. M., "Fibre Spinning," *Computational Analysis of Polymer Processing*, J. R. A. Pearson and S. M. Richardson, eds., Applied Science Pub., London and New York (1983).

Dheur, J., and M. J. Crochet, "Numerical Simulation of Coextrusion," 2nd Ann. Meet. Polymer Processing Soc., Montreal (Apr., 1986).

Dussan V., E. B., "The Moving Contact Line: The Slip Boundary Condition," *J. Fluid Mech.*, **77,** 665 (1976).

———, "Immiscible Liquid Displacement in a Capillary Tube: The Moving Contact Line," *AIChE J.*, **23,** 131 (1977).

———, "On the Spreading of Liquids on Solid Surfaces: Static and Dynamic Contact Lines," *Ann. Rev. Fluid Mech.*, **11,** 371 (1979).

Engelman, M. S., R. L. Sani, and P. M. Gresho, "The Implementation of Normal and/or Tangential Boundary Conditions in Finite-Element Codes for Incompressible Fluid Flow," *Int. J. Num. Meth. Fluids*, **2,** 225 (1982).

Han, C. D., *Multiphase Flow in Polymer Processing*, Academic Press, New York (1981).

Huebner, K. H., and E. A. Thornton, *The Finite-Element Method for Engineers*, Wiley, New York (1982).

Huh, C., and L. E. Scriven, "Hydrodynamic Model of Steady Movement of a Solid/Liquid/Fluid Contact Line," *J. Colloid Interface Sci.*, **35,** 85 (1971).

Joseph, D. D., M. Renardy, and Y. Renardy, "Instability of the Flow of Two Immiscible Liquids with Different Viscosities in a Pipe," *J. Fluid Mech.*, **141,** 309 (1984a).

Joseph, D. D., K. Nguyen, and G. S. Beavers, Non-Uniqueness and Stability of the Configuration of Flow of Immiscible Fluids with Different Viscosities," *J. Fluid Mech.*, **141,** 319 (1984b).

Kafka, F. Y., and E. B. Dussan V., "On the Interpretation of Dynamic Contact Angles in Capillaries," *J. Fluid Mech.*, **95,** 539 (1979).

Kistler, S. F., "The Fluid Mechanics of Curtain Coating and Related Viscous Free-Surface Flows with Contact Lines," Ph.D. Thesis, Univ. Minnesota, Minneapolis (1984).

Kistler, S. F., and L. E. Scriven, "Coating Flow Theory by Finite-Element and Asymptotic Analysis of the Navier-Stokes System," *Int. J. Num. Meth. Fluids*, **4,** 207 (1984).

Liaw, B. M., A. S. Kobayashi, and A. F. Emery, "Double-Noding Technique for Mixed-Mode Crack Propagation Studies," *Int. J. Num. Meth. Eng.*, **20,** 967 (1984).

Lowndes, J., "The Numerical Simulation of the Steady Movement of a Fluid Meniscus in a Capillary Tube," *J. Fluid Mech.*, **101,** 631 (1980).

Mavridis, H., A. N. Hrymak, and J. Vlachopoulos, "Finite-Element Simulation of Fountain Flow in Injection Molding," *Polym. Eng. Sci.*, **26,** 449 (1986).

Middleman, S., *Fundamentals of Polymer Processing*, McGraw-Hill, New York (1977).

Mirza, F. A., and M. D. Olson, "Energy Convergence and Evaluation of Stress Intensity Factor K_I for Stress Singular Problems," *Int. J. Fracture*, **14,** 555 (1978).

Mitsoulis, E., J. Vlachopoulos, and F. A. Mirza, "Numerical Simulation of Entry and Exit Flows in Slit Dies," *Polym. Eng. Sci.*, **24,** 707 (1984).

———, "Calendering Analysis without the Lubrication Approximation," *Polym. Eng. Sci.*, **25,** 6 (1985).

Nickell, R. E., R. I. Tanner, and B. Caswell, "The Solution of Viscous Incompressible Jet and Free-Surface Flows Using Finite-Element Methods," *J. Fluid Mech.*, **65,** 189 (1974).

Rose, W., "Fluid-Fluid Interfaces in Steady Motion," *Nature*, **191,** 242 (1961).

Silliman, W. J., and L. E. Scriven, "Separating Flow Near a Static Contact Line: Slip at a Wall and Shape of a Free Surface," *J. Comput. Phys.*, **34,** 287 (1980).

Southern, J. H., and R. L. Ballman, "Stratified Bicomponent Flow of Polymer Melts in a Tube," *Appl. Polym. Sci.*, **20,** 175 (1973).

———, "Additional Observations on Stratified Bicomponent Flow of Polymer Melts in a Tube," *J. Polym. Sci. Polym. Phys. Ed.*, **13,** 863 (1975).

———, "Preferential Wetting Phenomenon in Bicomponent Polymer Melt Flow," *J. Appl. Polym. Sci.*, **24,** 693 (1979).

Tanner, R. I., R. E. Nickell, and R. W. Bilger, "Finite-Element Methods for the Solution of Some Incompressible Non-Newtonian Fluid Mechanics Problems with Free Surfaces," *Comp. Meth. Appl. Mech. Eng.*, **6,** 155 (1975).

Tanner, R. I., *Engineering Rheology*, Oxford Univ. Press, New York (1985).

Taylor, C., and T. Hughes, *Finite-Element Modelling of the Navier-Stokes Equations*, Pineridge Press, Swansea (1981).

West, G. D., "On the Resistance to the Motion of a Thread of Mercury in a Glass Tube," *Proc. Roy. Soc. London, Ser. A*, **86,** 20 (1911).

Whitaker, S., *Introduction to Fluid Mechanics*, Prentice-Hall, Englewood Cliffs, NJ, 173 (1968).

Manuscript received Apr. 10, 1986, and revision received Sept. 23, 1986.